International Journal of Solids and Structures, 81, pp. 151-159 (2016) doi:10.1016/j.ijsolstr.2015.11.022

Identification of material properties using nanoindentation and surrogate modeling

Han Li[1], Leonardo Gutierrez[2], Hiroyuki Toda[1], Osamu Kuwazuru[3],Wenli Liu[3],Yoshihiko Hangai[4], Masakazu Kobayashi[5], and Rafael Batres[6*]

[1] Department of Mechanical Engineering, Kyushu University, Fukuoka, 819-0395, Japan.
[2] Plasess (Rumania) S.R.L., Timis, Romania 307221.
[3]Department of Nuclear Power and Energy Safety Engineering, University of Fukui, Fukui, 910-8507, Japan.
[4] Department of Intelligent Machines, Gunma University, Kiryu, Gunma, 376-8513, Japan.
[5] Department of Mechanical Engineering, Toyohashi University of Technology, Toyohashi, 441-8580, Japan.
[6] Escuela de Ingeniería y Ciencias, Tecnológico de Monterrey, Campus Cuernavaca, Mexico.

Abstract

In theory, identification of material properties of microscopic materials, such as thin film or single crystal, could be carried out with physical experimentation followed by simulation and optimization to fit the simulation result to the experimental data. However, the optimization with a number of finite element simulations tends to be computationally expensive. This paper proposes an identification methodology based on nanoindentation that aims at achieving a small number of finite element simulations. The methodology is based on the construction of a surrogate model using artificial neural-networks. A sampling scheme is proposed to improve the quality of the surrogate model. In addition, the differential evolution algorithm is applied to identify the material parameters that match the surrogate model with the experimental data. The proposed methodology is demonstrated with the nanoindentation of an aluminum matrix in a die cast aluminum alloy. The result indicates that the methodology has good computational efficiency and accuracy.

Keywords: nanoindentation; material properties; die cast aluminum alloy; surrogate model; finite-element analysis; optimization; neural networks; infill sampling criteria; differential evolution.

*Corresponding author, Rafael Batres, Email: rafael.batres@itesm.mx

1. Introduction

Contrasting to the conventional material development process, the ongoing project *Reverse 4D Materials Engineering* aims at rapid development of high-performance materials [1]. The objective of the project is to develop methods and tools that generate the optimum microstructure structure with a minimum computational effort. Such a challenge requires addressing reverse engineering problems and this paper is a first step towards that direction.

Determining material properties is crucial in the design of materials that are resistant to fatigue, wear, and other behaviors. Unfortunately, conventional mechanical methods are often destructive and complex. As an alternative, nanoidentation is a widely recognized technique that is relatively non-destructive and can be applied to small specimens for use in the measurement of mechanical properties of both bulk materials and thin coatings [2].

Much research has been done on methods that extract mechanical properties of materials from indentation tests. For example, Oliver and Pharr proposed an analytical method to nanoindentation-data to estimate hardness and elastic modulus [3]. Dao et al. proposed a reverse algorithm based on explicit equations that enables the extraction of elasto-plastic properties. In the same vein, Cao and Lu [4] extended the work of Dao et al. to spherical indentation. However, such methods are limited to certain parameters and materials.

Several authors have developed inverse algorithms based on finite element (FE) simulations to extract material properties. Some of these algorithms rely on methods that reduce the number of unknowns. For example, Cheng and Cheng [5], Ma et al. [6] and Heinrich et al. [7] use dimensional analysis for this purpose.

Surrogate modeling has been used as an approach to predict FE simulations. For example,

Heinrich et al. [8] proposed the method of Kriging to predict material properties from nanoindentation curves as an approach of curve fitting between experimental and numerical data. Other researchers used Artificial Neural Networks (ANNs) in which the inputs to the network are defined by the load-displacement response data and the desired outputs are the material parameters [9][10][11]. In their work, response curves are generated by finite element simulations for various parameter combinations in an attempt to match experimental data. However, these methods rely heavily on the finite element simulations which are expensive in terms of computation time. Furthermore, it becomes impractical when the number of parameters increases, since a large dimensional problem require a large number of simulations.

In general, surrogate models are constructed using data drawn from rigourous models (e.g. high-fidelity models), and provide a fast approximation of the original model, making optimization studies more efficient. Surrogate models have been successfully used in the design of aerospace devices [12], heat transfer devices [13], chemical process optimization [14], and combustion engine design [15].

In the field of material science and engineering, Jin et al. [16] used surrogate models combined with sharp indentation, dimensional analysis, and an energy method for calculating residual stress. The surrogate model was constructed as an Artificial Neural Network (ANN) that was trained with 240 finite element simulations, which were validated with other 40 simulations chosen randomly.

Haj-Ali et al. [17] developed ANN models trained with FE simulations for reproducing nanoindentation curves. However, only the loading part of the curve was used to generate the ANN models.

Theoretically, the application of an optimization technique directly to FE simulations can identify the material parameters. However, a typical optimization would require thousands of function evaluations, which would make this approach impractical. The problem is also complex because the nonlinearity from plasticity and large deformation adds non-convexity to the optimization problem. To cope with these issues, this paper proposes a using a combination of a sampling scheme, surrogate modeling, and a global optimization approach.

This paper describes the use of a surrogate modeling approach for determining material parameters with a small number of finite element simulations in an attempt to lower the computational cost.

The rest of this paper is organized as follows. Section 2 describes problem statement. The proposed methodology is presented in Section 3. Then, Section 4 discusses a case study to evaluate the proposed approach. Finally, Section 5 provides discussion and conclusions of this research.

2. Problem statement

The proposed approach employs surrogate modeling and a sampling method as the means to reduce the number of FE simulations. Specifically, we focus on the estimation of elastic and plastic parameters from load-displacement curves obtained from nanoindentation experiments. Therefore, the problem is formulated as the minimization of the objective function given in Equation 1, which is composed of two parts:

1. the error between the experimental load-displacement curve and the curve estimated by the surrogate model (first term in Equation 1); and

2. the difference between the areas under the experimental and estimated curves (second term in Equation 1).

$$\text{Minimize } \gamma_1 I_{\tilde{f}}(\tilde{\boldsymbol{p}}) + \gamma_2 \left| \int_{x_0}^{x_{final}} f(x, \boldsymbol{p}) dx - \int_{x_0}^{x_{final}} \tilde{f}\left(x, \tilde{\boldsymbol{p}}\right) dx \right| \quad (1)$$

Subject to:

$$g(x, \tilde{\boldsymbol{p}}) = 0, \quad (2)$$

where $\tilde{\boldsymbol{p}}$ is the decision variable which represents a vector of parameters whose values are known *a priori*; $\boldsymbol{p}$ is a vector of mechanical parameters which are intrinsically present in the material but whose range and values are initially unknown; $f(x_j, \boldsymbol{p})$ is the experimental indentation-load evaluated at depth (displacement) x_j; $\tilde{f}\left(x_j, \tilde{\boldsymbol{p}}\right)$ is the indentation-load calculated by the surrogate model at depth x_j; x is the depth of the indenter in the material (the known independent variable); x_0 is the initial value of x, and x_{final} is its last value; $I_{\tilde{f}}(\tilde{\boldsymbol{p}})$ is the root mean square error between the experimental curve and the curve estimated by the surrogate model, as calculated by Equation 11; and $\gamma_1$and γ_2 are weight parameters. Finally, the restriction $g(x, \boldsymbol{p})$ guarantees that the experimental and predicted responses overlap.

To convert the above constrained-problem into an unconstrained optimization problem, Equation (3) is added as a penalty function to Equation (1), resulting in:

$$\text{Minimize} \quad \gamma_1 I_{\tilde{f}}(\tilde{\boldsymbol{p}}) + \gamma_2 \left| \int_{x_0}^{x_{final}} f(x, \boldsymbol{p}) dx - \int_{x_0}^{x_{final}} \tilde{f}\left(x, \tilde{\boldsymbol{p}}\right) dx \right| + \gamma_3 \, h(g(x, \boldsymbol{p})) \quad (3)$$

where γ_3 is an additional weight parameter and $h(g(x, \boldsymbol{p}))$ is the penalty function.

If $g(x, \boldsymbol{p})$ represents the requirement to make the curves coincide at the point of maximum depth then $h(g(x, \boldsymbol{p}))$ can be expressed as:

$$h(g(x, \boldsymbol{p})) = \left| f(x, \boldsymbol{p}) \Big|_{x=x_{max}} - \tilde{f}(x, \tilde{\boldsymbol{p}}) \Big|_{x=x_{max}} \right| \tag{4}$$

where x_{max} the maximum depth of the indenter.

The problem of inferring the parameter vector $\boldsymbol{p}$ from the load-displacement response curves is ill-posed because of the existence of a large number of solutions. To solve this, a global optimization algorithm is applied.

In order to facilitate the quantification of the differences between the experimental data and the simulation, the experimental data is processed by decomposing the original data set into its loading and unloading segments (Figure 1). Then, in order to obtain continuous and noise-free curves, each segment is represented by

$$F_t = A_t (x + C_t)^{n_t} \tag{5}$$

where F_t is the experimental indentation load, x is the indentation depth, and A_t, C_t and n_t are parameters. Index t takes the value of 1 for the loading segment and the value of 2 for the unloading section. In order to account for the adjustment of the initial position of the indenter tip, an extra variable k is introduced that causes a shift of the curve along the abscissa (Figure 1).

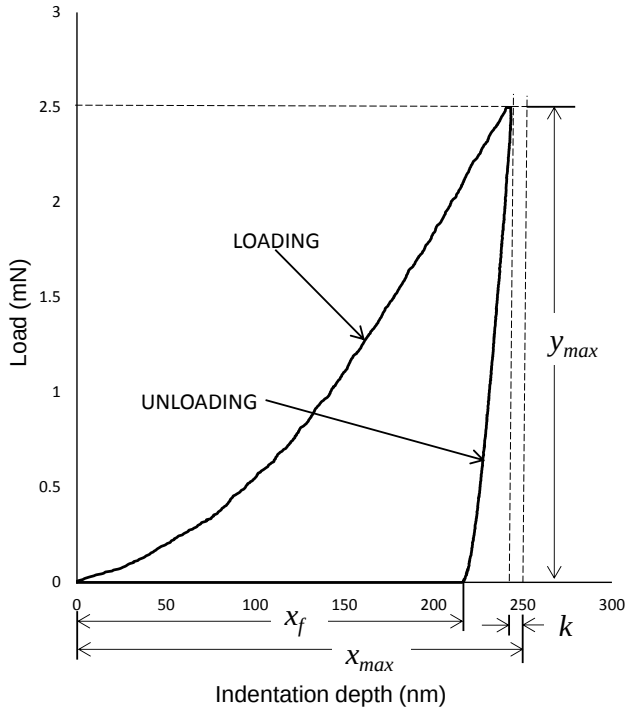

Figure 1. Indentation load-displacement curve

Thus, the experimental curve is represented as

$$\boldsymbol{F}(x,\boldsymbol{p}) = \begin{cases} A_1(x + C_1 + k)^{n_1}, & x \in [x_0, x_{max}] \\ A_2(x + C_2 + k)^{n_2}, & x \in [x_{max}, x_f] \end{cases} \tag{6}$$

where x_f is the final depth of the contact impression after unloading; x_{max} is the depth at the maximum indentation load in the FE simulation curve; and k is the post-experimental calibration.

The first part of the second term of Equation (1) can be approximated through an analytical integration of the power laws for each the load and unload segments of the experimental curve.

$$\begin{aligned} \int_{x_0}^{x_{final}} f(x,\boldsymbol{p})dx \\ \approx \int_{x0}^{xmax} A_1(x + C_1 + k)^{n1}dx \\ + \int_{xmax}^{xfinal} A_2(x + C_2 + k)^{n2}dx \end{aligned} \tag{7}$$

Since the actual maximum depth can be considered to occur at the intersection of the loading and unloading segments, the value of k can be obtained numerically by solving the following expression:

$$k = x_{max} - \min_x |A_1(x - C_1)^{n1} - A_2(x - C_2)^{n2}| \quad (8)$$

3. Methodology

An overview of the methodology is shown in Figure 2. The first step is to use a design-and analysis-of-computer-experiments (DACE) technique to generate a sampling plan that contains an initial set of sampling points. Next, rigorous simulations (FE simulations) are performed for each sample point, and a surrogate model is built based on these simulations. The next step is to optimize the objective function for a first estimation of the material properties. Then the methodology finds new points for model refinement. These new points are selected by means of an infill sampling criterion, which involves a second optimization step. Subsequently, a new surrogate model is generated, completing one iteration. The procedure is repeated until the termination criterion is reached[1]. The main elements of the methodology are explained in the following subsections.

3.1 Sampling plan

A finite number of sample points are needed to create a surrogate model. However, these points must be well-distributed in the design space. Thus, the initial population of sample points is obtained by means of design-and-analysis-of-computer-experiments (DACE) techniques

[1] In this paper, the stopping criterion is defined in terms of the number of iterations.

[18], which permit to fill evenly the design space with a limited number of points.

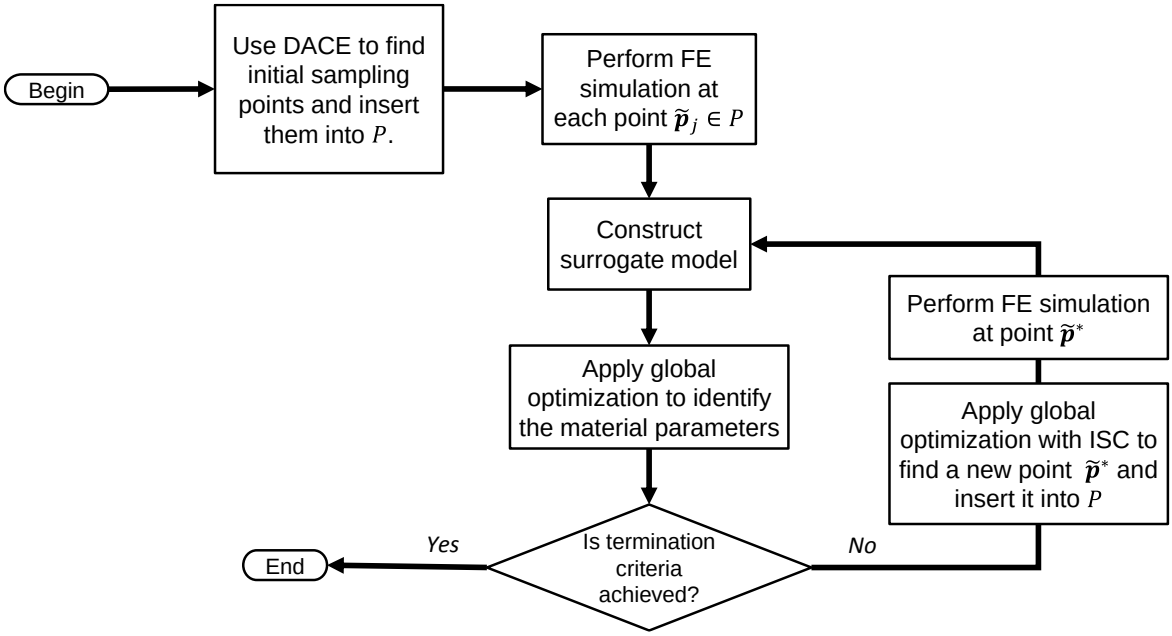

Figure 2. The proposed methodology.

The most frequently used techniques for DACE are: Latin hypercube design (LHS) [19], full-factorial design, orthogonal arrays, and Box-Behnken design. Each of these methods has its own advantages and disadvantages depending on the characteristics of the design problem. In this paper, the optimal LHS method [20] is utilized. Optimal LHS optimizes the sample plan according to the S-optimality criterion that aims at maximizing the mean distance from each design point to all the other points in the plan, so the points are as spread out as possible [21]. The advantage of this choice is that the design space can be divided uniformly for each parameter and guarantees to have good space-filling properties.

The sampling plan is then used as the basis for the simulation step. A rigorous simulation model is executed for all the values of the input variables in the sampling plan.

3.2 Surrogate model construction

A number of techniques are available for the generation of surrogate models. Polynomial regression [22], artificial neural networks [23] [24], radial basis function (RBF) [25], and Kriging [26][27] are among the most common. This paper employs artificial neural networks (ANN) as surrogate models. Note that in contrast with the work in [9][10][11], the proposed approach generates an ANN using the material parameters and the indentation depth as the input, and the load response as output.

Artificial neural networks are computational models inspired by the central nervous system, which are made of interconnected *neurons*. Typically, ANNs are composed of an input layer, one or more hidden layers and an output layer. The input layer is responsible for receiving a given input vector $\boldsymbol{x}$ and converts it to an output $\boldsymbol{y}(\boldsymbol{x})$ that becomes the input for another layer. A hidden layer converts the output from the previous layer by means of a transfer function.

Each neuron receives the input from all of the neurons in the preceding layer, multiplies each input by its corresponding weight factor $w_{i,j}$ and then adds a bias θ_j:

$$v_j = \sum w_{i,j} y_i + \theta_j \tag{9}$$

where v_j is the total or net input and y_i is the input from the i^{th} neuron in the preceding layer.

A neuron in the network produces its output y_j by processing the net input through a transfer function h. In this work, the log-sigmoid function (Equation (10)) is used as transfer

function, except for the last hidden layer that implements a linear transfer function ($y_j = h(v_j) = v_j$).

$$y_j = h(v_j) = \frac{1}{1+e^{-v_j}} \tag{10}$$

An ANN is trained by a set of known inputs and outputs. In this paper, this training set is obtained from FE simulations. During the training process, the neural network gradually learns the relationship of interest by modifying the values of the weighting factors and biases to minimize the error between the actual and predicted outputs of the training set.

The number of hidden layers can be found through performance measures. Although, performance measures such as the mean square error are common for evaluating model accuracy, due to risk of overfitting the model with a large number of hidden layers, the preferred performance measures are the Schwarz's Bayesian Criterion (SBC) [28], and the corrected Akaike's Information Criterion (AIC) [29].

3.3 New point selection

The success of finding the global optimum is influenced by the number and location of the sample points. As shown in Figure 2, a new point is added at each iteration until the stopping criteria is reached. The selection of the new point is determined by an infill sampling criterion (ISC). Several infill sampling criteria have been proposed for Kriging surrogate models, including the expected improvement (EI) [30], the probability of improvement (PI) [31], lower confidence bounding [32], maximization of predicted error [33], and conditional minimizer entropy [34].

This paper proposes an ISC that searches areas of high estimated error between the prediction of the surrogate model and the experimental data. In addition, it also considers the spatial position of the design variables.

The proposed ISC is based on an offset (error) function $I_f(\tilde{\boldsymbol{p}})$ which is a quality index based on the difference between the experimental curve and the curve estimated by the surrogate model. This offset function is given by Equation (11):

$$I_f(\tilde{\boldsymbol{p}}) = \sqrt{\frac{1}{m}\sum_{j=1}^{m}\left(f(x_j,\boldsymbol{p}) - \tilde{f}(x_j,\tilde{\boldsymbol{p}})\right)^2} \tag{11}$$

where $\tilde{\boldsymbol{p}}$ is a possible sampling point, $f(x_j,\boldsymbol{p})$ is the experimental indentation-load evaluated at depth x_j, $\tilde{f}(x_j,\tilde{\boldsymbol{p}})$ is the indentation-load calculated with the current surrogate model at depth x_j, and m is the number of experimental data of the load-displacement curve.

In order to avoid adding a new point to a location too close to an existing point, the following weight function is introduced.

$$w(\tilde{\boldsymbol{p}},\tilde{\boldsymbol{p}}_i) = 1 - \exp(-|\tilde{\boldsymbol{p}} - \tilde{\boldsymbol{p}}_i|^2) \tag{12}$$

where $\tilde{\boldsymbol{p}}$ is a candidate for a new point, and $\tilde{\boldsymbol{p}}_i$ is an existing point.

Based on the above equations, the new sampling point $\tilde{\boldsymbol{p}}^*$ is the point $\tilde{\boldsymbol{p}}$ that maximizes the following expression:

(13)

$$\sum_{i=1}^{n} w(\tilde{\boldsymbol{p}}, \tilde{\boldsymbol{p}}_i)(I_f(\tilde{\boldsymbol{p}}) - I_f((\tilde{\boldsymbol{p}}_i))$$

where n is the number of current sampling points. Given the current surrogate model, an optimization algorithm is applied to find $\tilde{\boldsymbol{p}}^*$. Figure 3 uses a fictitious unidimensional model to illustrate the new point selection in the context of the proposed methodology.

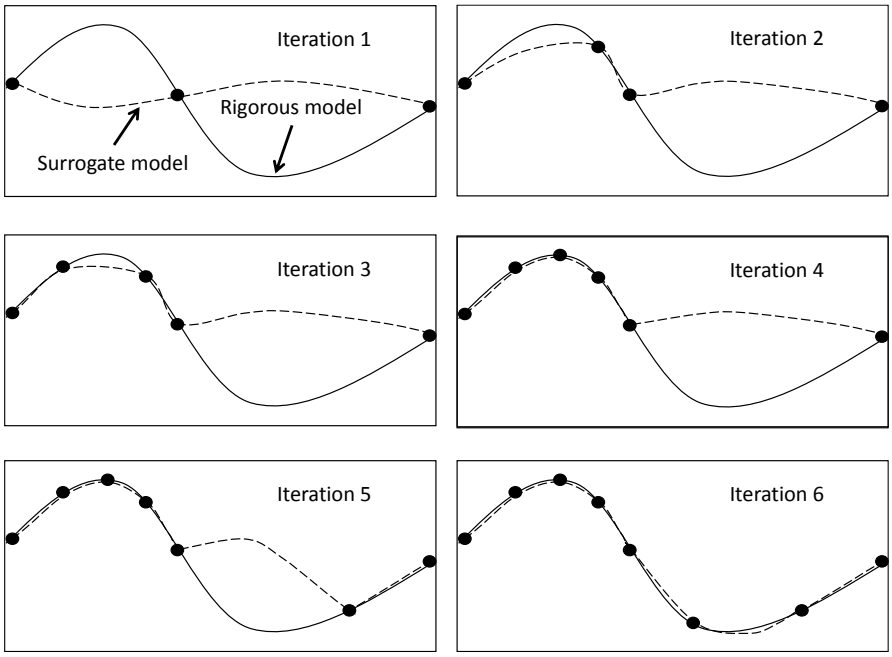

Figure 3. Illustration showing the selection of new points within the process of the surrogate model construction.

4. Case study

Indentation experiments were carried out with an Elionix ENT-1100 nanoindentation machine which is capable of loads between 98μN and 980mN, with measurements between 0 and 20 μm. A triangular pyramid Berkovich tip was used as indenter.

The material used in the experiment was a JIS ADC12 die cast aluminum alloy. To enlarge

the metallographic structure, after cutting the material out of the product of high-pressure die casting, it was melted in a steel cup and solidified by furnace-cooling. The ingot was cut to a square specimen of 10 mm width and 1 mm thick. The surface of specimen was mirror-polished and underwent the nanoindentation tests. Only the aluminum matrix was investigated in this paper.

The nanoindentation test was carried out as a load-controlled experiment. Additionally, the indenter maximum load was set to 2.5 mN. The indentation was directed to the interior of aluminum grain, and forty points were measured from many grains. One representative result was selected by choosing the hardness nearest to the average hardness among the forty results. The experimental load-displacement curve for a representative result is shown in Figure 1. The experimental curves were fitted to Equation 6, with a RMSE of 0.01650 and a coefficient of determination of 0.9995.

The parameters to be determined are the elastic and plastic constants of the aluminum matrix in line with the isotropic material. The elastic constants are the Young's modulus E and Poisson's ratio ν, but the latter is set to 0.3 and assumed constant. For simplicity, we employed the Swift equation as a hardening model (Equation 14).

$$\sigma_Y = C(\propto +\varepsilon_P)^n \tag{14}$$

where σ_Y is the current yield stress, ε_P the equivalent plastic strain, and C, α, and n are fitting constants. Consequently, the objective is to determine four constants: E, C, α, and n. However, the proposed identification method is not limited to the Swift equation and other hardening models can be used.

4.1 Finite element model

An axisymmetric finite-element model was developed using the MSC Marc/Mentat® software [35]. The indenter is approximated by a conical indenter with a tip angle of 70.3 degrees, which was set to make the relationship between indentation depth and contact surface area equal to the Berkovich indenter. The specimen and indenter were modeled as a deformable body with homogeneous and isotropic material properties, using the von Mises yield criterion and the Swift hardening model. The FE model assumes isotropic hardening. The diamond indenter was assumed to be elastic[2], and its Young's modulus and Poisson's ratio were set to 1140 GPa and 0.07, respectively. The model used 15849 three-node triangular-elements (with a minimum size of 5 nm) and 8194 nodes. The three-node triangular element is used to discretize both the specimen and indenter. The model also considered geometric nonlinearities. In each simulation, loading and unloading used 200 increments each. The Newton-Raphson method was used to solve the finite-element equations. Figure 4 illustrates the general model setup and mesh of the indenter and the specimen.

[2] For computational accuracy, a deformable body was used for modeling the diamond indenter in order to account for the behavior in the initial stage of contact characterized by a small contact area and high stress concentration.

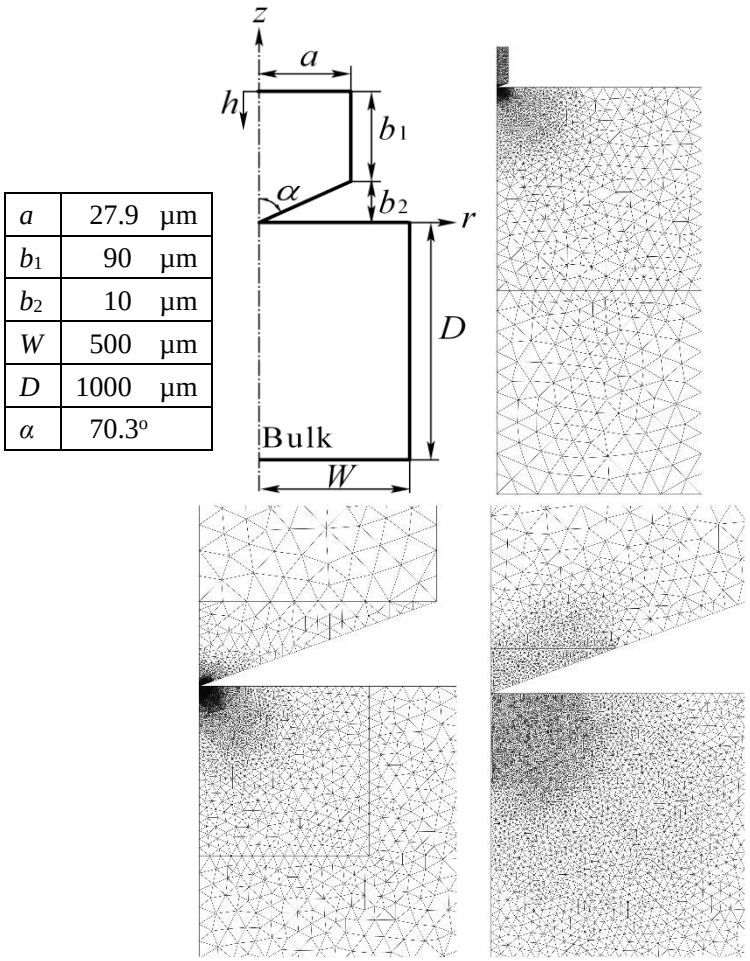

a	27.9	μm
b_1	90	μm
b_2	10	μm
W	500	μm
D	1000	μm
α	70.3°	

Figure 4. Axisymmetric analysis model and finite element discretization.

The indenter is pushed vertically into the plane surface of the specimen following the experimental data. The contact analysis was carried out without friction between the specimen and the indenter. However, friction can be easily considered in the proposed identification methodology.

Each simulation took between 30 and 45 minutes on a HP Intel Xeon W3680 workstation (3.33GHz) with a single core.

4.2 Sampling plan

The initial sampling was performed with the optimal LHS method as explained in Section

3.1. The ranges of the parameters used for the optimization are shown in Table I, and the initial sampling-plan is shown in Table II. Each sample point yields to one simulation.

TABLE I: RANGES OF THE PARAMETERS

Parameters	E (GPa)	C (MPa)	N	α
Lower Limit	50	500	0.1	0
Upper Limit	150	1500	0.3	0.002

TABLE II: INITIAL SAMPLING PLAN OBTAINED WITH LHS

Sample points	E (GPa)	C (MPa)	N	α
1	52.192	598.413	0.2025	0.001289
2	93.952	945.308	0.1812	0.000460
3	127.304	693.983	0.2846	0.000883
4	104.503	779.996	0.1394	0.001733

4.3 Artificial Neural Network development

The ANN was trained with a set that consisted of several points identified by the sampling scheme. The inputs to the artificial neural networks consisted of numeric values of: the four parameters (E, C, n, α); depth x (the independent variable); and an auxiliary binary variable d that distinguishes the loading (d=0) and unloading (d=1) sections of the indentation curve for all the sampling points. The output of the artificial neural network was the corresponding

indentation load. As shown in Table III, each sampling point *i* consists of *m* groups of parameter values, where each group is organized as (x_{ij}, E_i, C_i, n_i, α_i, d) with output L_{ij}, where *m* represents the number of experimental points in a single load-displacement curve.

The data used for training consisted of FE simulation results (one simulation for each sample point). The ANNs were created using the Neuroet toolbox [36].

TABLE III: STRUCTURE OF THE INPUTS AND OUTPUTS FOR ANN TRAINING

Inputs						Outputs
x	E	C	n	α	d	L
x_{11}	E_1	C_1	n_1	α_1	0	L_{11}
x_{12}	E_1	C_1	n_1	α_1	0	L_{12}
⋮	⋮	⋮	⋮	⋮	⋮	⋮
x_{1m}	E_1	C_1	n_1	α_1	1	L_{1m}
x_{21}	E_2	C_2	n_2	α_2	0	L_{21}
x_{22}	E_2	C_2	n_2	α_2	0	L_{22}
⋮	⋮	⋮	⋮	⋮	⋮	⋮
x_{2m}	E_2	C_2	n_2	α_2	1	L_{2m}
⋮	⋮	⋮	⋮	⋮	⋮	⋮

Based on the performance evaluation, both the Schwarz's Bayesian Criterion, and the corrected Akaike's Information Criterion suggested that the most accurate models were obtained with 6−12 hidden layers. Visual inspection permitted to identify that 8 hidden layers was the best number of layers. More than 8 hidden neurons resulted in over-fitting the data, while fewer than 8 hidden neurons resulted in a poor model fit. Training was carried out with standard back propagation. Furthermore, the transfer function between the input layer and the hidden layer was log-sigmoid, while the transfer function between the last hidden layer and the output layer was pure-linear.

In the ANN generation, each set of simulation data was decomposed into a training set (80% of the data), a test set (10% of the data) and a validation set (10% of the data). The training set was used to find the weighting factors and biases of the hidden layers. After training the ANN, its predictive capabilities were evaluated using the test set, which is a data set that were not used in training. Finally, the validation set was used in the process of finding the number of hidden layers.

4.4 Optimization

An integrated environment was developed with interfaces to the experimental data and artificial neural network models. The integrated environment (RIoMP) was implemented using the R statistical environment and is available for research purposes[3] (Figure 5).

The weight parameters of Equation (3) were set to $\gamma_1 = 0.8$ and $\gamma_2 = \gamma_3 = 0.1$.

The nonlinearity of the objective function and the possibility of non-uniqueness of the solution makes the inverse problem a non-convex optimization problem. Therefore, a robust global optimization method was required. In this case study, the Differential Evolution algorithm (DE) [37] was used due to its robustness and computational efficiency and the fact that it has been found to solve a large number of problems.

DE aims at solving an objective function of the form:

$$\min f(\boldsymbol{x}) \qquad \forall \boldsymbol{x} \in \mathbb{R}^d \tag{15}$$

where $\boldsymbol{x}$ is a *d*-dimensional parameter vector and $f(\boldsymbol{x})$ is an objective function. DE requires a set of n parameter vectors known as population. Each iteration updates a population

[3] Available at: http://campus.cva.itesm.mx/rbatres/riomp.html

using a set of operators to lead the next generation.

The mutation operator chooses three members of the population x_{r_1}, x_{r_2}, and x_{r_2} to generate a new parameter vector according to Equation (16):

$$v_i = x_{r_1} + F(x_{r_2} - x_{r_3}) \quad (16)$$

where F is a weighting factor. The parameters of the mutated vector are then mixed with the parameters of another vector of the population called the target vector. This parameter mixing, known as crossover, generates a new vector called the trial vector. If the trial vector yields to a lower value of the objective function, the trial vector replaces the target vector in the next generation; otherwise the target vector remains in the next population. This process continues for a fixed number of generations or until a termination criterion is satisfied.

Specifically, we used the R[4] package DEoptim [38]. The parameters of the DE algorithm were as follows: population size = 40, CR (probability of crossover) = 0.5, weighting factor F = 0.8, and number of generations = 200.

For each sample point, the optimization was performed 10 times and the best result was selected, with each optimization taking about 4 minutes.

[4] R is a free software environment for statistical computing and graphics. Available at: https://www.r-project.org/

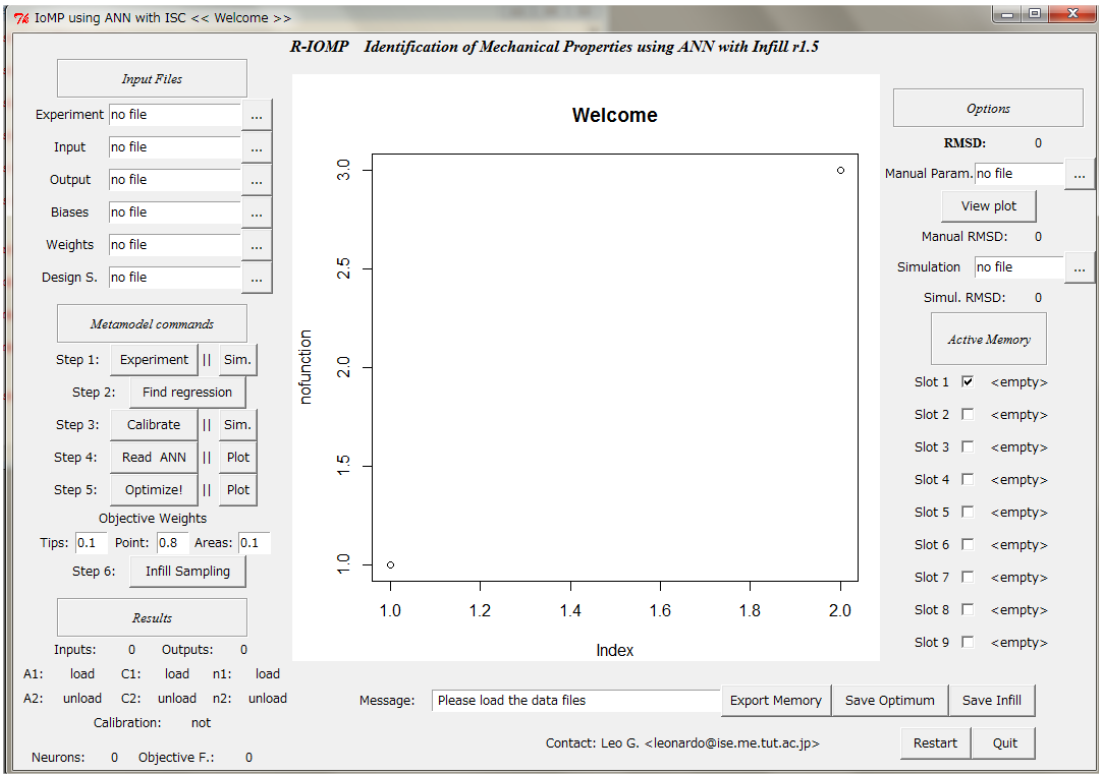

Figure 5.GUI of the RIoMP toolbox.

4.5 Results and discussion

Analysis of the quantitative adequacy of the model showed that the model adequately described the finite-element simulation data in all the iterations. The RMSE and r^2 were used as measures of goodness-of-fit. An average RMSE of 0.05998 and an r^2 of 0.9991 demonstrated the adequacy of the surrogate model to replicate the finite-element model. The goodness-of-fit was also qualitatively verified by visual inspection of the nanoindentation curves. Table IV contains the final values of the parameters obtained with a surrogate model of 24 sampling points.

TABLE IV: ESTIMATED VALUES OF THE PARAMETERS

E (GPa)	C (MPa)	N	α
86.83	743.73	0.107	0.00062

Figure 6 compares the load-displacement curve obtained with the surrogate model against the experimental curve. Similarly, Figure 7 compares the load-displacement curve obtained with the finite-element model against the experimental curve. In both cases, the final values of the parameters were used.

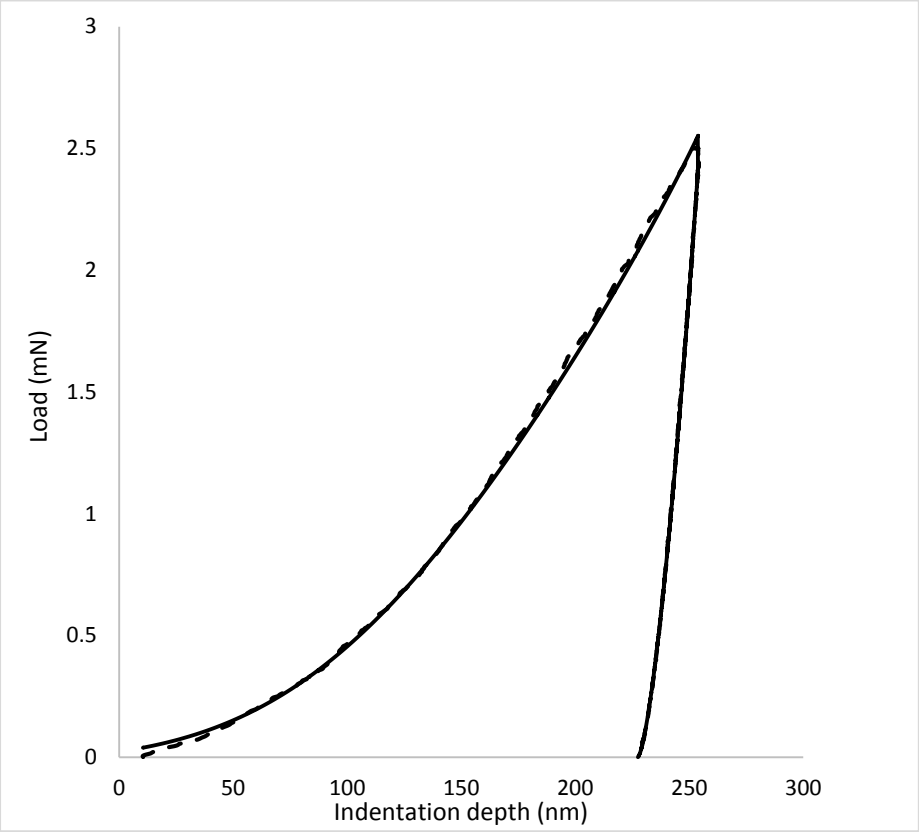

Figure 6. The load-displacement curve obtained with the surrogate model using the estimated parameters of Table III. The dotted line indicates the experimental curve. Zero load at zero displacement is not observed because the experimental curve was calibrated to account for initial contact errors.

As explained by Forrester [39], the r^2 between the surrogate model output and the experimental data can be used as a measure of the accuracy of the shape of the

nanoindentation curve obtained by the surrogate model. Figure 8 shows the convergence of the predictive capabilities of the surrogate model. It can be seen that the surrogate model assumes a characteristic shape early in the convergence, which was verified by visually inspecting the load-displacement curve obtained by the surrogate model.

The root mean square errors (RMSE) between the finite element model output and the experimental data are shown in Figure 9. The results show that convergence is also achieved from the point of view of the accuracy of the finite-element model.

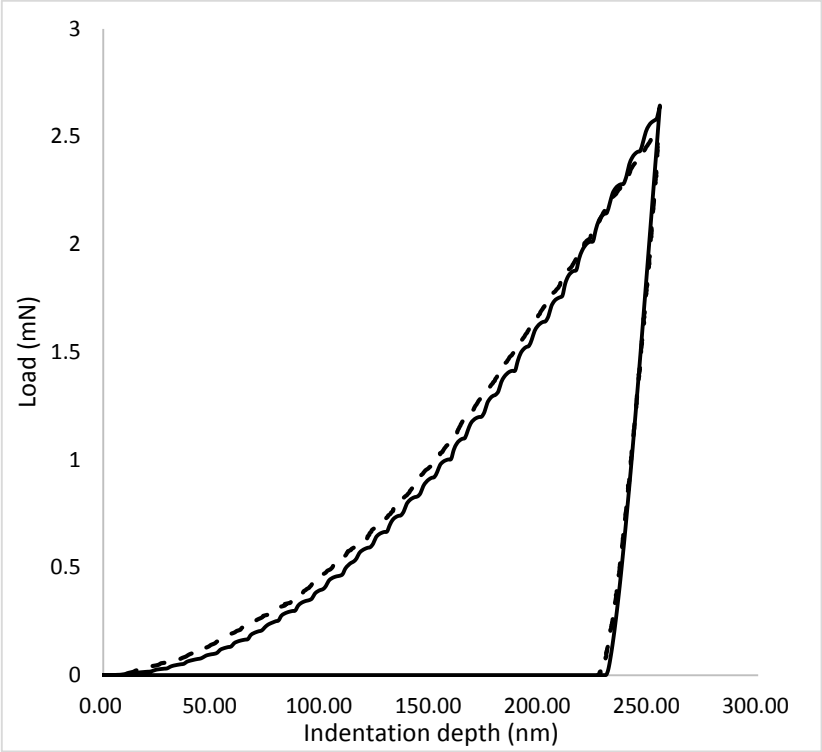

Figure 7. The load-displacement curve obtained with the finite-element model using the estimated parameters of Table III. The dotted line indicates the experimental curve.

Figure 10 shows that convergence is achieved quickly for the elastic modulus E, the strain-hardening coefficient C, and the strain-hardening exponent n. However, the strain constant α presents a more erratic behavior probably due to the low sensibility of the

parameter in the established range that results in little influence on the model output.

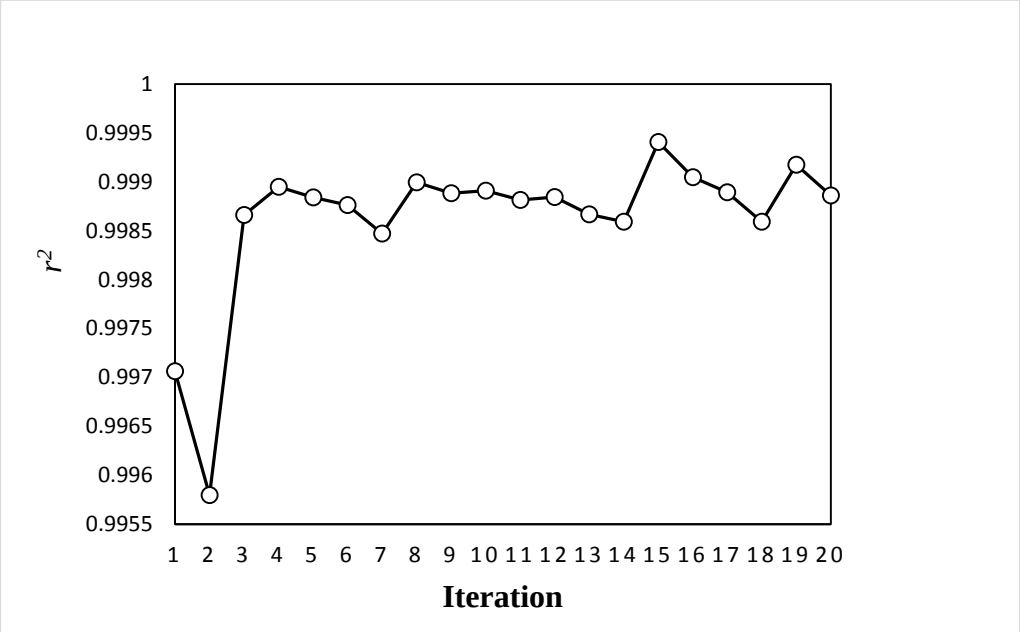

Figure 8. Convergence of r^2 for the surrogate model.

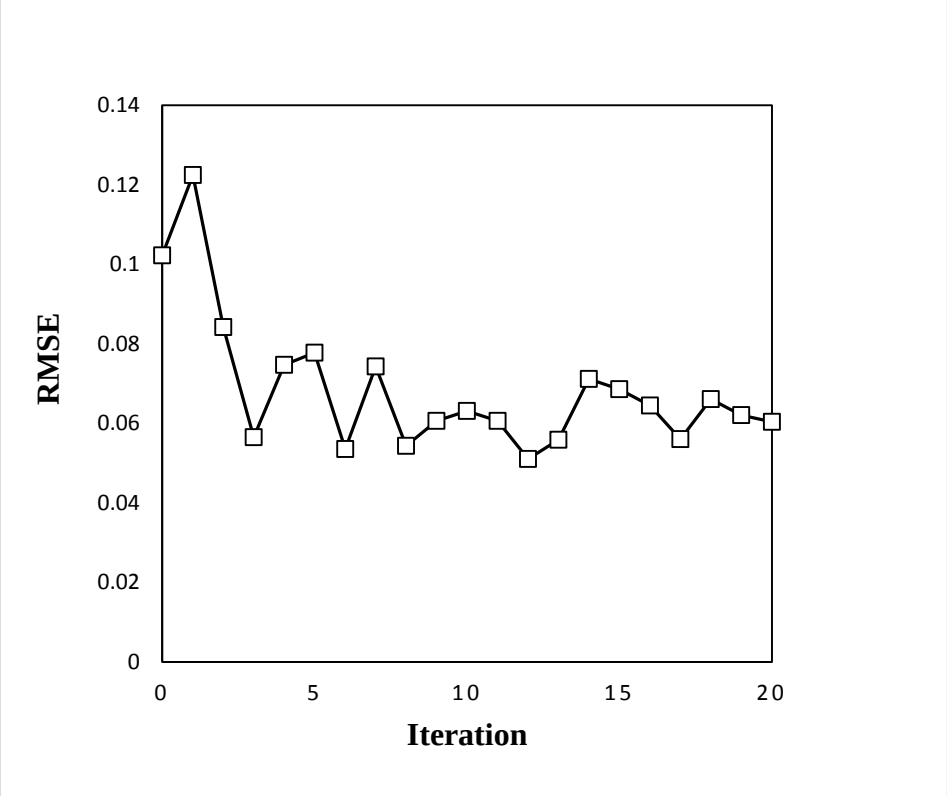

Figure 9. Convergence of RMSE error for the finite-element model

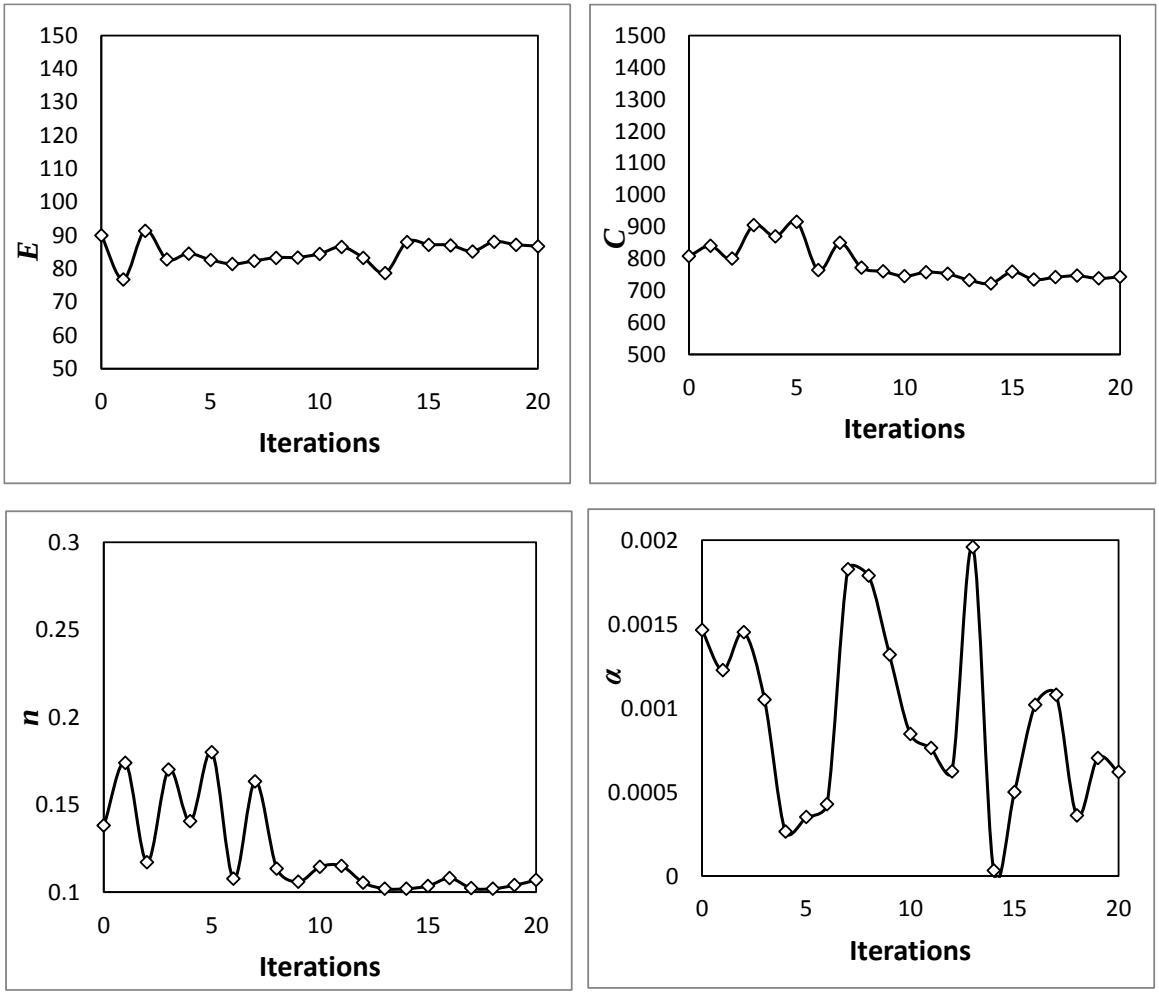

Figure 10. Convergence of the parameters for aluminum AC4CH-T6.

5. Conclusion and future work

In this paper, an optimization methodology using artificial neural networks was developed for the estimation of mechanical properties of materials. A case study was presented for the estimation of four parameters of an aluminum matrix obtained from a nanoindentation load-displacement curve with a small number of computer simulations. Compared to traditional methods in which hundreds of finite-element simulations are carried out, the results show that the proposed method is one order of magnitude faster.

Further work is necessary to account for the sensibility of the parameters in order to

improve accuracy of the method. In addition, more must be done to account for flexibility in the design space. At present, the boundaries of the design space were fixed based on expert opinions. One possible approach would be the use of the previous optimization result to resize the design space.

It is worth mentioning that the nanoindentation data is highly dependent on the crystal orientation. In this study, an experimental data of intermediate hardness was employed for the identification. In the simulation, although the material was assumed to be isotropic, a material such as single crystal aluminum must be considered anisotropic. This will be addressed in future research.

Acknowledgment

This work was undertaken partly with the support of a Grant-in-Aid for Scientific Research (S) from JSPS, through Subject No. 24226015. The authors gratefully acknowledge the help of Dr. Akihide Hosokawa and Dr. Vinicius Aguiar de Souza. Finally, the authors are indebted to the reviewers and editor of the International Journal of Solids and Structures for their time and effort, and for their kind comments that greatly improved the manuscript.

References

[1] H. Toda, R. Batres, O. Kuwazuru, M. Kobayashi, A. Hosokawa. Reverse 4D materials engineering: Its framework and recent evolution. J. Jpn. Inst. Light Met. 64 (2014) 518–524.

[2] F.M. Haggag, J.A. Wang, T.J. Theiss, Using Portable/In-Situ Stress-Strain Microprobe System to Measure Mechanical Properties of Steel Bridges During Service, SPIE, 2946 (1996) 65–75.

[3] W.C. Oliver, G.M. Pharr, An improved technique for determining hardness and elastic modulus using load and displacement sensing indentation experiments, J. Mater. Res. 7 (1992) 1564–1583.

[4] Y.P. Cao, J. Lu, A new method to extract the plastic properties of metal materials from an instrumented spherical indentation loading curve, Acta Mater. 52 (2004) 4023–4032.
[5] Y.T. Cheng, Z.M. Zheng, Scaling, dimensional analysis, and indentation measurements, Mater. Sci. Eng. R-Rep. 44 (2004) 91–149.
[6] Z.S. Ma, Y.C. Zhou, S.G. Long, C.S. Lu, An inverse approach for extracting elastic-plastic properties of thin films from small scale sharp indentation, J. Mater. Sci. Technol. 28 (2012) 626–635.
[7] C. Heinrich, A.M. Waasa, A.S. Wineman, Determination of material properties using nanoindentation and multiple indenter tips, Int. J. Solids Struct. 46 (2009) 364–376.
[8] C. Heinrich, A.M. Waas, A.S. Wineman, Measuring the matrix in-situ properties of fiber reinforced composites using nanoindentation − A virtual experiment, 1st Joint Canadian & American Technical Conference American Society of Composites (CACSMA), Sep. 15−17, University of Delaware (2009).
[9] N. Huber, I. Tsagrakis, C. Tsakmakis, Determination of constitutive properties of thin metallic films on substrates by spherical indentation using neural networks, International Journal of solids and structures, 37(44) (2000) 6499–6516
[10] N. Huber, C. Tsakmakis, Determination of constitutive properties from spherical indentation data using neural networks. Part I: the case of pure kinematic hardening in plasticity laws, Journal of the Mechanics and Physics of Solids, 47(7) (1999) 1569–1588
[11] N. Huber, and C. Tsakmakis, A new loading history for identification of viscoplastic properties by spherical indentation, J. Mater. Res., 19 (2004) 101–113
[12] N.V. Queipo, R.T. Haftka, W. Shyy, T. Goel, R. Vaidyanathan, P. K. Tuckerb, Surrogate-based analysis and optimization, Prog. Aerosp. Sci. 41 (2005) 1–28.
[13] Z. Qian, C. C. Seepersad, V. R. Joseph, J. K. Allen, C. F. J. Wu, Building Surrogate Models based on detailed and approximate Simulation, J. Mech. Des. 128 (2006) 668–677.
[14] J. A. Caballero, I. E. Grossmann, Rigorous flowsheet optimization using process simulators and surrogate models, AIChE Journal 54 (2008) 2633–2650.
[15] S. Jakobsson, M. Saif-Ul-Hasnain, R. Rundqvist, F. Edelvik, B. Andersson, M. Patriksson, M. Ljungqvist, D. Lortet, K. Wallesten, Combustion engine optimization: A multiobjective approach, Optim. Eng. 11 (2010) 533–554.
[16] H. Jin, W. Yang, L. Yan, Determination of residual stresses and material properties by an energy-based method using artificial neural networks, P. Est. Acad. Sci. 61(2012) 296–305.
[17] R. Haj-Ali, H.K. Kim, S.W. Koh, A. Saxena, R. Tummala, Nonlinear constitutive models from nanoindentation tests using artificial neural networks, Int. J. Plasticity 24(2008) 371–396.
[18] M.D. Mackay, R.J. Beckman, W.J. Conover, A comparison of three methods for selecting values of input variables in the analysis of output from a computer code, Technometrics, 21 (1979) 239–245.
[19] D. Bursztyn, D.M. Steinberg, Comparison of Designs for Computer Experiments, J. Stat. Plan. Infer. 136 (2006) 1103–1119.
[20] R. Stocki, A method to improve design reliability using optimal Latin Hypercube sampling. Computer Assisted Mechanics and Engineering Sciences 12, (2005) 87–105.
[21] E. Läuter, Experimental design in a class of models, Mathematische Operationsforschung und Statistik, 5 (1974) 379–398.

[22] A. I. Khuria, M. Conlona, Simultaneous Optimization of Multiple Responses Represented by Polynomial Regression Functions, *Technometrics*, 23 (1981) 363-375.
[23] A. J. Skinner, J. Q. Broughton, Neural networks in computational materials science: training algorithms, Model. Simul. Mater. Sc. 3 (1995) 371–390.
[24] A. Cichocki, R. Unbehaven, Neural Networks for Optimization and Signal Processing, 1st ed. Chichester, U.K.: Wiley, Ch. 2, (1993) 45–47.
[25] N. Dyn, D. Levin, S. Rippa, Numerical procedures for surface fitting of scattered data by radial basis functions, SIAM J. Sci. Stat. Comput. 7 (1986) 639–659.
[26] J. B. Sacks, W.J. Welch, Designs for Computer Experiments, *Technometrics* 31 (1989) 1–47.
[27] J. B. Sacks., W. J. Welch, T.J. Mitchell, H. P. Wynn, Design and Analysis of Computer Experiments, Stat. Sci. 4 (1989) 409–435.
[28] G. Schwarz, Estimating the dimension of a model. The Annals of Statistics, Vol. 6, No. 2 (1978), 461–464.
[29] H. Akaike, A new look at the statistical model identification. IEEE Transactions on Automatic Control, Vol. 19 (6) (1974) 716–723.
[30] D. R. Jones, M. Schonlau, W. J. Welch, Efficient global optimization of expensive black-box function, J. Global Optim. 13 (1998) 455–492.
[31] F. A. C. Viana, R. T. Hafika, Surrogate-based optimization with parallel simulations using the probability of improvement, AIAA, (2010) 2010–9392.
[32] D. Cox, and S. John, SDO: A Statistical Method for Global Optimization, Proceedings of the ICASE/NASA Langley Workshop on Multidisciplinary Optimization (Alexandrov, N. M. and Hussaini, M. Y., eds.), Hampton, VA, SIAM, (1995) 315–329.
[33] J. Liu, Z. Han,W. Song, Comparison of infill sampling criteria in kriging-based aerodynamic optimization, 28th Int. Congress Aeronaut. Sci. Brisbane, Australia, (2012) 23–28.
[34] D. Geman, B. Jedynak, An active testing model for tracking roads in satellite images, Tech. Rep. 2757, Institut National de Recherche en Informatique et en Automatique (INRIA) (1995).
[35] MSC, Marc 2010 Volume A: Theory and User Information, MSC Software Corporation, (2010).
[36] A.P. Noble, H.E. Tribou, Neuroet: An easy-to-use artificial neural network for ecological and biological modeling, Ecol. Model. 203 (2007) 87–98.
[37] K.V. Price, R. M. Storn, J. A. Lampinen, Differential Evolution – A Practical Approach to Global Optimization. Berlin Heidelberg: Springer–Verlag. ISBN 3540209506 (2006).
[38] D. Ardia, K. Boudt, P. Carl, K. M. Mullen, B. G. Peterson, Differential Evolution with DEoptim. An Application to Non-Convex Portfolio Optimization. The R Journal, 3(1), (2011) 27–34
[39] A. I. Forrester, N. W. Bressloff, and A. J. Keane, Optimization Using Surrogate Models and Partially Converged Computational Fluid Dynamics Simulations, Proceedings of the Royal Society of London, Series A: Mathematical and Physical Sciences, 462, (2000), 2177–2204